Numerical Investigation of Focused Waves and their Interaction with a Vertical Cylinder using REEF3D

Hans Bihs[1]*, Mayilvahanan Alagan Chella[1], Arun Kamath[1], Øivind Asgeir Arntsen[1]
[1]Department of Civil and Environmental Engineering
Norwegian University of Science and Technology (NTNU), 7491 Trondheim, Norway

Journal of Offshore Mechanics and Arctic Engineering, 2017, **139** , pp. 1-19.

Abstract

For the stability of offshore structures, such as offshore wind foundations, extreme wave conditions need to be taken into account. Waves from extreme events are critical from the design perspective. In a numerical wave tank, extreme waves can be modeled using focused waves. Here, linear waves are generated from a wave spectrum. The wave crests of the generated waves coincide at a preselected location and time. Focused wave generation is implemented in the numerical wave tank module of REEF3D, which has been extensively and successfully tested for various wave hydrodynamics and wave-structure interaction problems in particular and for free surface flows in general. The open-source CFD code REEF3D solves the three-dimensional Navier-Stokes equations on a staggered Cartesian grid. Higher order numerical schemes are used for time and spatial discretization. For the interface capturing, the level set method is selected. In order to test the generated waves, the time series of the free surface elevation are compared with experimental benchmark cases. The numerically simulated free surface elevation shows good agreement with experimental data. In further computations, the impact of the focused waves on a vertical circular cylinder is investigated. A breaking focused wave is simulated and the associated kinematics are investigated. Free surface flow features during the interaction of non-breaking focused waves with a cylinder and during the breaking process of a focused wave are also investigated along with the numerically captured free surface.

Keywords:

Focused waves, wave structure interaction, focused wave forces

---

*Corresponding author, hans.bihs@ntnu.no

Postprint, published in Journal of Offshore Mechanics and Arctic Engineering, doi: http://dx.doi.org/10.1115/1.4036206

1 Introduction

Extreme waves are large waves at sea and their interaction with a structure exerts a large hydrodynamic load on it. They emerge from nonlinear wave-wave interaction in an irregular sea state when the waves coincide in their phase at one point in space and time. Although the occurrence of extreme waves is rare, they can cause severe damage to offshore and coastal structures. A notable example is the extreme wave event with a peak crest elevation of 18.5 m that occurred in the central North Sea at Statoil Draupner platform in 1995. There are many such events reported regarding sinking of ships and extreme damage to structures due to the impact of high and steep focused waves Stansell (2004). In order to understand the behavior of extreme steep waves, knowledge about the generation, kinematics, propagation characteristics, probability of occurrence and environmental conditions is essential Soomere (2010). Focused waves can be defined as a superpositioning of many small amplitude waves focused at a point using linear wave theory. When the wave amplitude increases, linear theory breaks down and it cannot be applied for steep waves. The application of second order wave models is also limited. Hence, the complete description of extreme steep waves can only be possible with a nonlinear higher-order model.

Modeling of extreme wave conditions with a random wave series is more demanding as it requires long simulation times. However, an extreme wave can be represented using the evolution of a dispersive focusing wave group. Baldock et al.Baldock et al. (1996) showed that the physical process close to the focusing point is highly nonlinear due to the complex wave-wave interactions. They also reported that the complexity of the evolution of wave group increases for larger waves and decreases for larger spectral bandwidths. The knowledge concerning the characteristics and kinematics of extreme waves is critical for understanding the physical processes and the associated higher-order load effects on structures, e.g. ringing Chaplin et al. (1997).

Bai and Eatock Taylor (2007) studied the interaction of non-linear regular waves and focused waves with a large vertical cylinder using a higher-order boundary element method together with the domain decomposition technique. The numerical results were in good agreement with the experimental data for the regular wave propagation and the diffraction force on the cylinder. However, the numerical results for focused waves and forces were not validated against experimental data. In addition, the application of the model was limited to the modeling of non-breaking waves propagating in constant water depth. They also noticed numerical instabilities for the simulation of large amplitude incident waves due to the wave non-linearity.

Ning et al. Ning et al. (2009) performed experimental and numerical investigations on the evolution of the focused groups and the underlying kinematics. A numerical method based on a higher-order boundary element method (HOBEM) was used. Comparison between numerical and experimental results was presented for the free surface elevations and the water particle velocities. The authors pointed out that the 2-nd order wave components play an important role in defining the local steepening of the focused wave crest. It was concluded that wave-wave interaction strongly influences the evolution of the focused wave groups up to the 3rd order harmonics, which directly affect the focusing process. Zang et al. Zang et al. (2010) carried out physical experiments on the interaction of breaking and non-breaking steep waves with a fixed vertical cylinder. The focused waves were generated in the laboratory using the localized wave groups approach. The authors investigated the free surface deformation around the cylinder and the horizontal forces on it for different wave conditions.

Several numerical simulations based on computational fluid dynamics (CFD) attempted to model focused waves and the interaction with a vertical fixed cylinder. Westphalen et al. Westphalen et al. (2012) modeled extreme focused waves using the commercial CFD packages CFX and STAR-CCM+. The wave forces on a horizontal and a vertical cylinder were also calculated and compared with experimental data. Paulsen et al. Paulsen et al. (2014) performed numerical simulations of phase-focused waves over a constant water depth and their interaction with slender cylinders using a fully nonlinear-coupled solver. They combined a fully nonlinear potential solver with the Navier- Stokes solver OpenFOAM. Chen et al. Chen et al. (2014) numerically investigated the interaction of focused waves with a vertical circular cylinder using OpenFOAM. The nonlinear interaction of focused wave groups with a vertical cylinder was well represented in the numerical simulation.
The main aim of the present paper is to investigate focused wave generation, kinematics and the interaction with a vertical circular cylinder with the open-source CFD model REEF3D Bihs et al. (2016*a*). REEF3D has been successfully used for simulations of breaking wave kinematics Alagan Chella et al. (2015a); Alagan Chella et al. (2016*b*), breaking wave forcesBihs et al. (2016*b*); Alagan Chella et al. (2016*a*); Kamath et al. (2016), ocean wave energy devices Kamath et al. (2015*b*) and sediment transport under wave conditions Afzal et al. (2015). In the present study, the main focus is to implement focused wave generation, simulate both non-breaking and breaking focused waves and study their interaction with a vertical cylinder. Compared previously presented numerical models, the present numerical model uses higher order numerical schemes for temporal and spatial discretizations together with a ghost cell immersed boundary method on a staggered Cartesian grid. First, the numerical model is validated for simulating focused waves and their interaction with a vertical cylinder against the experimental data in Ning et al. (2009) and Zang et al. (2010). The computed results are in good agreement with the experimental data for free surface elevations and wave forces. Further, the study investigates breaking focused waves and their interaction with a vertical cylinder. The free surface flow features during the interaction of non-breaking and breaking focused waves with a vertical cylinder are presented and the important characteristics are discussed.

2 NUMERICAL MODEL

2.1 Governing equations

The governing equations for the fluid calculations in the open-source CFD code REEF3D Bihs et al. (2016*a*) are the continuity and the incompressible Navier-Stokes equations, which ensure mass and momentum conservation:

$$\frac{\partial u_i}{\partial x_i} = 0 \tag{1}$$

$$\begin{aligned}\frac{\partial u_i}{\partial t} + u_j \frac{\partial u_i}{\partial x_j} = &-\frac{1}{\rho}\frac{\partial p}{\partial x_i} \\ &+ \frac{\partial}{\partial x_j}\left[\nu\left(\frac{\partial u_i}{\partial x_j} + \frac{\partial u_j}{\partial x_i}\right)\right] + g_i\end{aligned} \tag{2}$$

where $i, j = 1, 2, 3$. u_i is the mean velocity component, t time, x_i is the spatial directions, ρ is the water density, p is the pressure, ν is the kinematic viscosity and g is the gravity.

Since the pressure cannot be solved directly from the Navier-Stokes equations, Chorin's projection method Chorin (1968) for incompressible flow is employed. Here, Eq. 2 is solved, the pressure is neglected in the first step and the intermediate velocity u_i^* is computed. The Poisson equation for the pressure is formed by calculating the divergence of the intermediate velocity field.

$$-\frac{\partial}{\partial x_i}\left(\frac{1}{\rho\left(\phi^n\right)}\frac{\partial P}{\partial x_i}\right) = -\frac{1}{\Delta t}\frac{\partial u_i^*}{\partial x_i} \tag{3}$$

ϕ^n is the density location. The Poisson equation is solved using the parallelized Jacobi-preconditioned BiCGStab algorithm van der Vorst (1992). The pressure is then used to correct the velocity field, making it divergence free.

The calculation of wave propagation based on the solution of the Navier-Stokes equations can be challenging, because it can suffer from numerical diffusion, which consequently leads to an unphysical damping of the waves. So, the order of accuracy of the discretization methods requires special attention. At the same time, numerical stability and efficiency cannot be neglected. In the REEF3D, these requirements are balanced by the selection of the fifth-order WENO (weighted essentially non-oscillatory) scheme in the conservative finite-difference framework Jiang and Shu (1996) for the convection discretization of the flow velocities. The overall WENO discretization stencil consists of three local ENO-stencils. These stencils are weighted depending on their smoothness, with the smoothest stencil contributing the most. The level set function ϕ is discretized by the Hamilton-Jacobi version of the WENO scheme Shu (1997). With the fifth-order WENO scheme for convection discretization, accurate solutions can be obtained without artificially high air velocities impacting the quality of the free surface. In particular, this scheme provides numerical solutions with higher order accuracy, ensuring good numerical stability with non-oscillatory performance near the interface, i.e. discontinuities which is essential for modeling free surface ocean waves. Also, this scheme can handle large gradients right up to the shock very accurately by taking local smoothness into account. Consequently, an accurate representation of wave propagation and transformation can be achieved together with the third-order TVD Runge-Kutta scheme for the time discretization.

For time, a fractional step method is used Le and Moin (1991), based on the third-order accurate TVD Runge-Kutta scheme Shu and Osher (1988). Instead of solving the Poisson equation for the pressure after every Euler sub-step, only one Poisson equation needs to be solved after the last sub-step. After the first two sub-steps, the intermediate velocities are corrected with the pressure from the previous time step. For the typically small time steps used in wave simulations, this approach delivers very acceptable accuracy, similar to solving the Poisson equation after each sub-step. Adaptive time stepping with a CFL number of 0.1 is used for the simulations in this paper.

All cases are run on a Cartesian grid, which results in a high grid quality with uniform cell spacings and aspect ratios. The solution variables have a staggered grid arrangement with in a cell. The velocity variables are defined at the center of the cell faces, while the level set function and the pressure at the cell centers. This ensures tight velocity-pressure coupling, avoiding unphysical oscillations of the flow velocities. At the same time, the location of the velocities and pressure with respect to the free surface is consistent with the definition of the density.

Complex solid boundaries of the solution domain are handled with the local directional

ghost cell immersed boundary method (GCIBM). The solution for the flow field is extrapolated into the solid by updating fictitious ghost cells. Here, the ghost cell extrapolation is carried out separately for each coordinate component. Using object oriented programming techniques, the implementation accounts for ghost cells that are updated from multiple directions as well. Further details regarding the numerical model are presented in Bihs et al. (2016). As a result, no explicit boundary treatment is required within the various discretization schemes. As an additional benefit of this method, the generation of high-quality grids becomes trivial. The current three-dimensional implementation of the algorithm is based on the local directional approach by Berthelsen and Faltinsen Berthelsen and Faltinsen (2008). Ghost cells are also used within the implemented domain decomposition framework for the parallelization. These ghost cells are updated with the values from the neighboring processors via MPI (Message Passing Interface).

2.2 Level Set Method

The wave propagation problems in the current paper are modeled as two-phase fluid flow systems. The free surface is modeled as the interface between the two fluids water and air. For the capturing of the interface, the level set method is used Osher and Sethian (1988). The level set function is fully differentiable in space with standard numerical discretization methods. This gives the possibility for using high-order methods for the temporal and spacial treatment of the interface capturing scheme. The level set function $\phi(\vec{x},t)$ defines the smooth signed distance away from the interface, with the zero-level set representing the free surface. This results in the following relationships:

$$\phi(\vec{x},t)\begin{cases} > 0 \; if \; \vec{x} \in phase \; 1 \\ = 0 \; if \; \vec{x} \in \Gamma \\ < 0 \; if \; \vec{x} \in phase \; 2 \end{cases} \tag{4}$$

The Eikonal equation $|\nabla\phi| = 1$ is valid throughout the solution domain. The interface can be moved under an externally generated velocity field by solving the following convection equation:

$$\frac{\partial\phi}{\partial t} + u_j\frac{\partial\phi}{\partial x_j} = 0 \tag{5}$$

When the interface evolves, the level set function can become distorted. In order to regain the signed-distance property, which also improves mass conservation, the level set function is reinitialized after each time step. Here, a PDE based reinitialization scheme is used Sussman et al. (1994).

2.3 Numerical Calculation of Wave Forces

Forces in the numerical model are computed as follows. The pressure and the wall shear stress are integrated over the surface Ω of the structure of interest. This happens in a discrete fashion, evaluating the pressure P and the normal component of the wall shear stress tenspr τ for each of the cell surfaces of the structure:

$$F = \int_\Omega (-\mathbf{n}P + \mathbf{n}.\tau)d\Omega \tag{6}$$

Because the Navier-Stokes equations in Eqn. (2) are solved including the gravity term, the pressure resulting from the projection method includes the hydrostatic part in addition to the

dynamic effects. As a result, it is the total force acting on a structure that is determined by Eqn. (6).

3 FOCUSED WAVE GENERATION

For the simulations in the present paper, the waves were generated with a simple Dirichlet inlet boundary conditions. Usually relaxation zone style wave generation is prefered due to the better wave quality Alagan Chella et al. (2015a) and for the better absorption when structures are placed in the wave tank Bihs et al. (2012)Kamath et al. (2015*a*). While in the current cases, a vertical structure is placed in the tank, the focused wave group is of relatively short time, and it is expected that the reflections traveling back from the structure will not the effect the wave generation. For the numerical beach, the relaxation method Mayer et al. (1998) is employed in all cases.

The focused wave generation method is based on the irregular wave generation by superpositioning of the linear regular waves components. The 1st-order free surface, $\eta^{(1)}$ is defined as:

$$\eta^{(1)} = \sum_{i=1}^{N} A_i cos\theta_i \tag{7}$$

where, A_i is the amplitude of each wave component and θ_i is the phase of each component, which is defined as:

$$\theta_i = k_i x - \omega_i t - \epsilon_i \tag{8}$$

where ω_i is the angular frequency and k_i is the wave number of each component. ϵ_i is the phase angle of each wave, and for irregular waves this is random. In the case of focused waves, ϵ is chosen in such a way that each individual wave focuses at a specified time t_F and location x_F.

$$\epsilon_i = k_i x_F - \omega_i t_F \tag{9}$$

Using linear superposition, the amplitude of each wave component can be expressed in terms of the wave spectrum $S_i(\omega)$ and the amplitude at the focus point A_F:

$$A_i = A_F \frac{S_i(\omega)\Delta\omega}{\sum_{i=1}^{N} S_i(\omega)\Delta\omega} \tag{10}$$

The amplitude of each wave component in the wave group is determined by multiplying the amplitude at the focus point (A_F) with the autocorrelation function of the free surface elevation. Here, the contribution of each spectral component to the maximum wave height at the focus point is obtained. In the present study, the JONSWAP spectrum is used for the generation of the irregular waves. The measured spectrum in the sea can be approximated by the various semi-empirical forms, which correspond to the locally generated waves. The required significant wave height H_s, the peak angular frequency ω_p and the number of components N are given as input values to the JONSWAP spectrum:

$$S_i(\omega) = \frac{5}{16} H_s^2 \omega_p^4 \omega_i^{-5} (-\frac{5}{4}) exp((\frac{\omega_i}{\omega_p})^{-4}) \gamma^{exp(\frac{-(\omega-\omega_p)^2}{2\sigma^2{\omega_p}^2})} A_\gamma \tag{11}$$

The frequency spectrum, $S_i(\omega)$ gives the distribution of the wave energy as a function of angular frequency ω. The first-order horizontal velocity $u^{(1)}$ and the vertical velocity $w^{(1)}$ are defined as the sum individual wave components:

$$u^{(1)} = \sum_{i=1}^{N} A_i \omega_i \frac{cosh(k_i(z+d))}{sinh(k_i d)} cos\theta_i \tag{12}$$

$$w^{(1)} = \sum_{i=1}^{N} A_i \omega_i \frac{sinh(k_i(z+d))}{sinh(k_i d)} sin\theta_i \tag{13}$$

With the relatively high wave steepnesses in the present study, it is necessary to obtain second-order focused waves which take into account the wave-wave interaction. Here, the second-order component is added to first-order component of the free surface elevation and the velocities:

$$\eta = \eta^{(1)} + \eta^{(2)} \tag{14}$$

$$u = u^{(1)} + u^{(2)} \tag{15}$$

$$w = w^{(1)} + w^{(2)} \tag{16}$$

As in Ning et al. Ning et al. (2009), the second-order wave components are implemented using second-order irregular wave theory Schäffer (1996) .

4 RESULTS

4.1 Focused Wave Kinematics

In order to validate the focused wave generation and propagation in REEF3D, numerical results are compared with experimental data. At first, data in Ning et al. (2009) for the wave kinematics of focused waves in the wave tank without any structure is investigated. The experiments were performed in a 69 m long and 3 m wide flume. The focus location was 11.4 m away from the wave paddle. At this location x_F, a wave gage was located. The data from this wave gage is used in the current study for comparison with the numerical model. The water depth was $h = 0.5$ m for all cases. In the numerical model, the focus point x_F is chosen to be 7.5 m away from the inlet location. The smaller value for x_F is chosen for computational efficiency . The focus point is still far enough from the wave generation zone to test the capability of the numerical model to represent the focus wave propagation process correctly. In the numerical simulations, a total of 20 regular wave components are used to generate focused waves in the wave tank. Compared to other numerical studies of the same casesWestphalen et al. (2012)Ning et al. (2009), the focus point is chosen significantly further away from the paddle location in order to study the focused wave propagation. Since the cases in this subsection are symmetric across the channel width, the numerical calculations are performed in two dimensions (2D). The total numerical tank length is 15 m. Due to the difference in the length of the numerical wave tank, the experimental free surface results are shifted in time to match the numerical focus time, but this is kept consistent for all comparisons. From the experimental data Ning et al. (2009), cases A and B are simulated (see Table 1). The 2D cases with a maximum of 24000 grid cells have been run on a 4-core laptop. For case A, the amplitude of the focused wave is $A_F = 0.0313$ m. The comparison for the free surface elevation at the focus point x_F between the numerical and experimental

No.	T [s]	A_F [m]	x_F	t_F	x_{Fa}	t_{Fa}
Case A	1.2	0.0313	7.5	10.0	7.55	10.05
Case B	1.25	0.0875	7.2	10.0	8.50	10.55

Table 1: Simualtions cases for focused wave generation and propagation Ning et al. (2009). x_{Fa} and t_{Fa} are the actual focus distance and time.

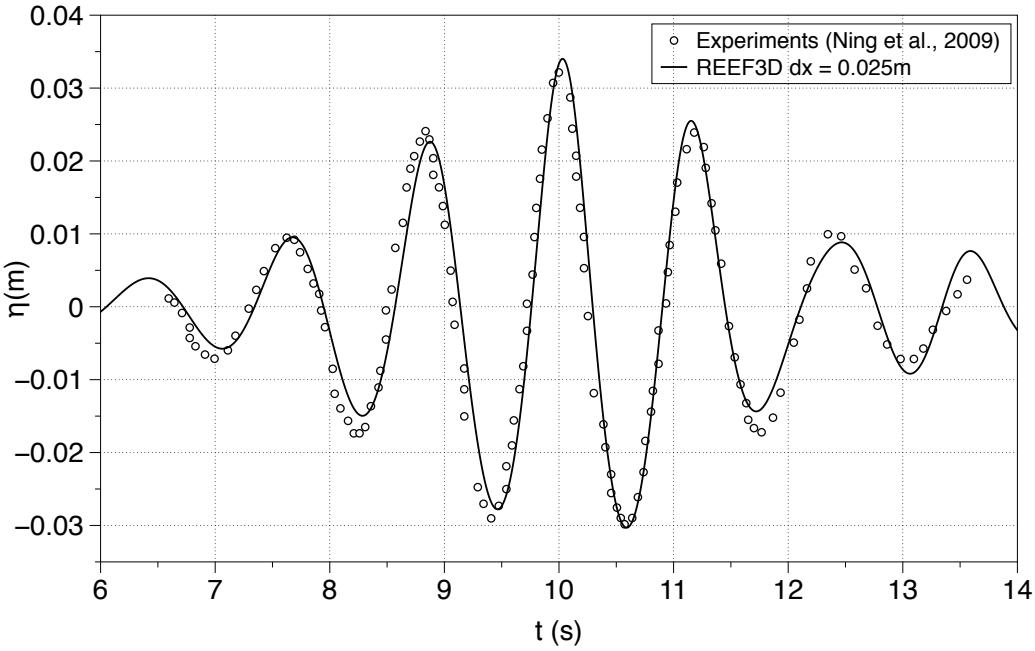

Figure 1: Comparison of the numerical results with the experimental wave gauge data at the focus point X_F for case A as in Ning et al. (2009).

results is shown in Fig. 1. It can be seen that the numerical model is capable of predicting the magnitude of the focused wave very well. For this case, wave non-linearity plays a minor role and the results are obtained at the intended focus point and time. Fig. 2 presents the free surface elevation for dx=0.075, 0.05, 0.025, 0.01m. It appears that the laboratory waves are reproduced well in the numerical simulations with dx=0.025m and 0.01m. However, the grid size dx=0.025m is computationally a good choice for simulations. Based on this, the following simulations will use $dx = 0.025$ m.

For the case B, the wave amplitude is higher than in the first case. Thus, higher wave non-linearity is expected in this case. Fig. 3 shows the free surface elevations along the numerical wave flume for the given focus time $t_F = 10.0$ s and for the time $t = 10.55$ s, at which the highest wave crest occurs at $x = 8.5$ m. This observation is inline with previous studies Westphalen et al. (2012)Ning et al. (2009). For cases of higher wave steepness and resulting higher non-linearity, the focus point is shifted further downstream. In Fig. 4, the wave surface elevation for the linear input focus point $x_F = 7.2$ m and the actual focus point at $x = 8.5$ m are compared with the experimental data. The simulated free surface elevation

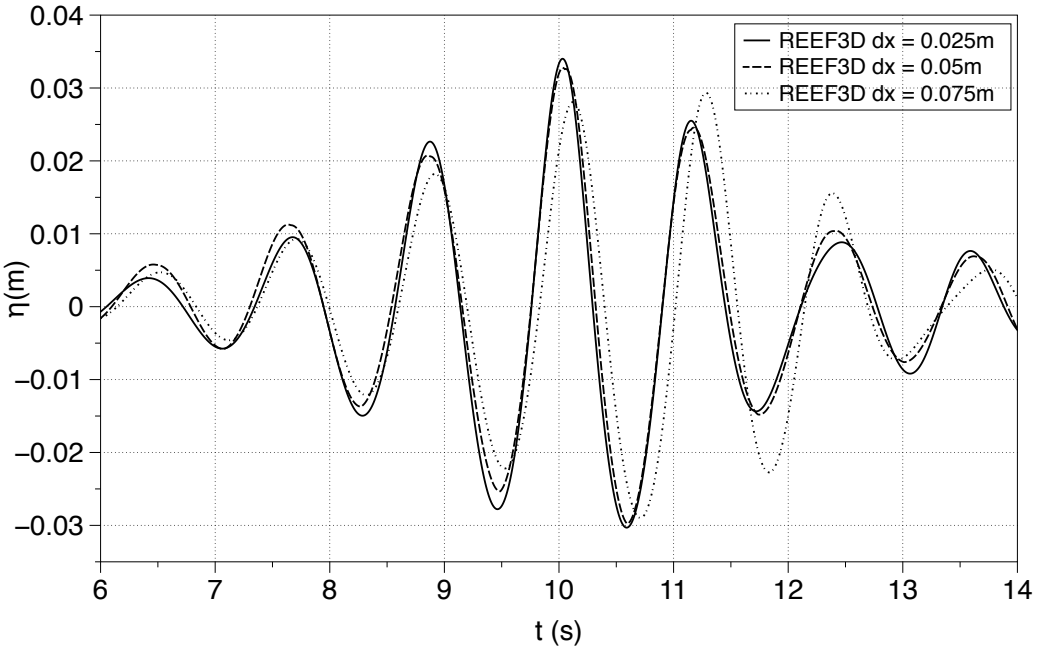

Figure 2: Numerical grid refinement study for case A.

for the actual focus point at x=8.5 m is in good agreement with the experimental data which is shifted by 0.55 s in time scale.
The difference in the focus point between the experiment and the numerical simulation occurs primarily due to the higher order wave components which evolve during the interaction of steep wave components. This effect has already been reported by Baldock et al. (1996), Westphalen et al. (2012) and Ning et al. (2009). In the present study, the second-order focused wave components are simulated with second-order irregular wave theory (scäffer et al. 1996) for steep waves. It is observed from the numerical results that focus point shifts further downstream for steeper waves due to the nonlinear wave-wave interaction. The wave non-linearity increases with the increasing wave amplitude. In particular, it is difficult to preserve the energy in a group of steep waves during its evolution without breaking in the numerical wave tank. In addition, the nonlinear interactions of steep wave components make this group evolution process even more difficult to model. Thus, the higher order wave components becomes more prominent to describe the physical process.

4.2 Non-Breaking Focused Wave-Structure Interaction

In order to investigate the focused wave-structure interaction, three-dimensional simulations are performed with a vertical circular cylinder located in the tank for the experiments by Zang et al. Zang et al. (2010). The experiments were performed in a shallow water basin (35 m x 25 m) with a water depth of 0.505 m. The cylinder with the diameter $D = 0.25$ m was placed 7.8 m away from the wave generation paddles and its upstream side coincides with the focus point. Two different cases are chosen with different values for A_F as listed in Table 2. Similar to the cases in the previous subsection, the wave steepness and the contribution of the non-linear wave components differentiate the two cases. In the numerical setup, the

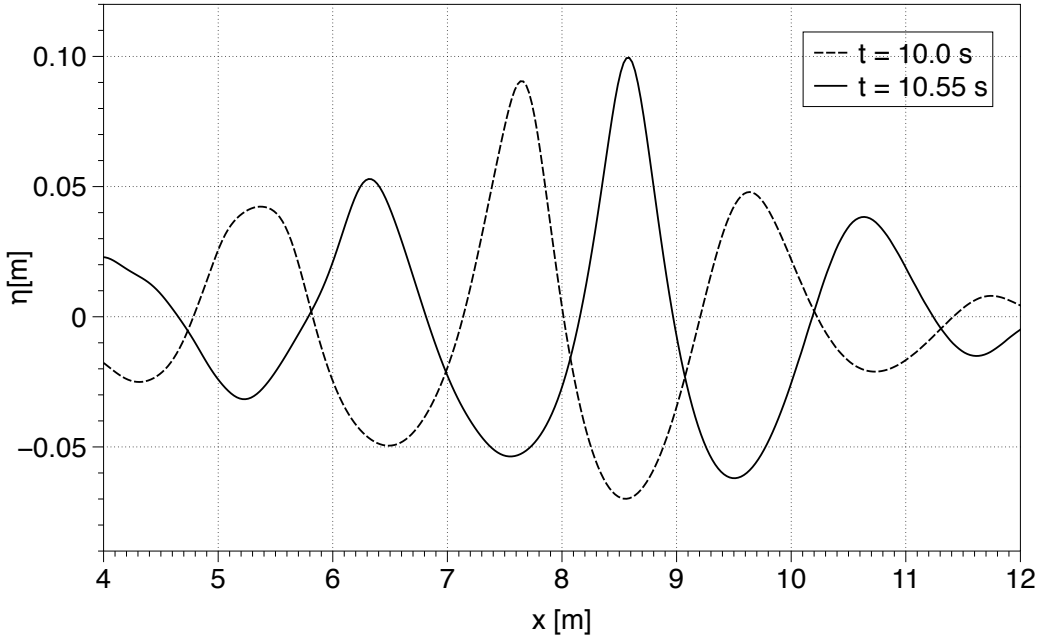

Figure 3: Free surface elevations along the wave flume, in wave direction for case B.

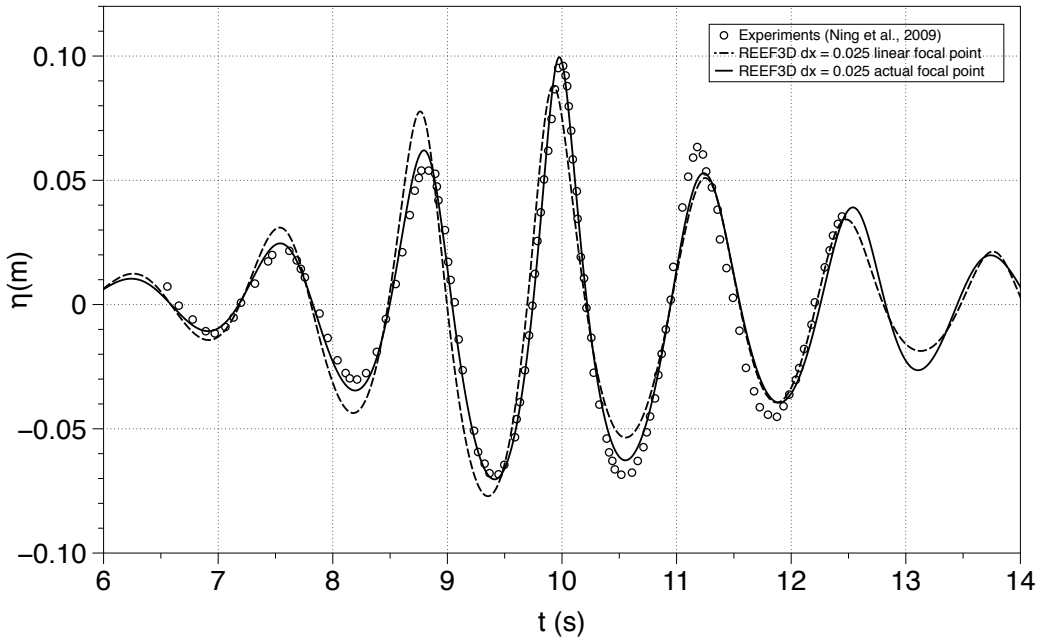

Figure 4: Comparison of the numerical results with the experimental wave gauge data at the focus point X_F for case B as in Ning et al. (2009).

No.	T [s]	A_F [m]	x_F [m]	t_F [s]
Case C	1.22	0.035	5.35	8.0
Case D	1.22	0.07	5.35	8.0

Table 2: Simulation cases for the focused wave-structure interaction as in Zang et al. (2010)

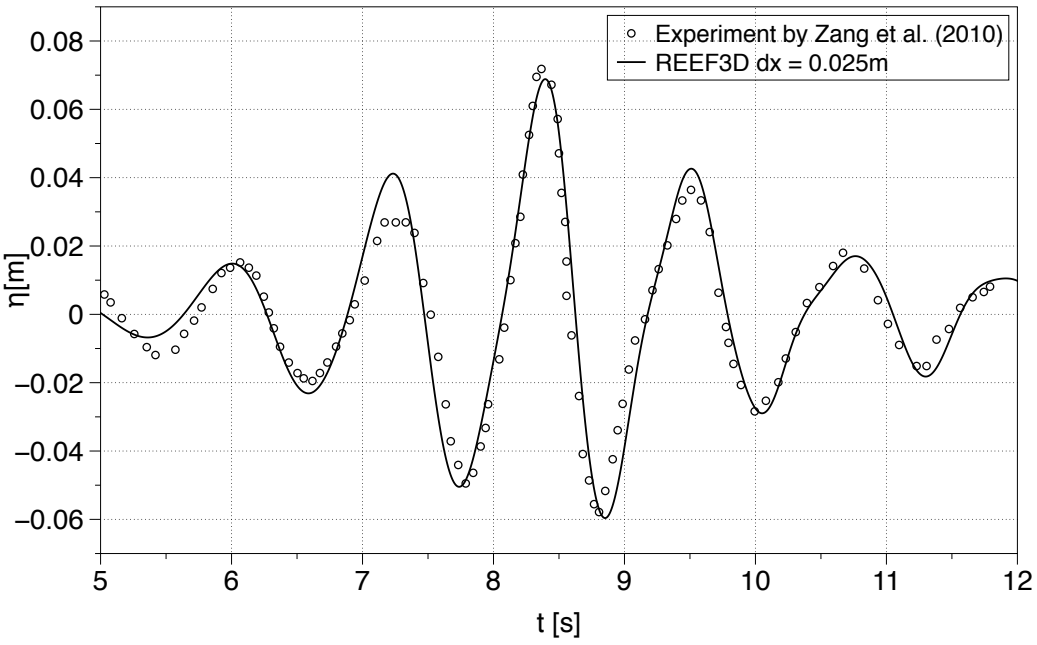

Figure 5: Comparison of numerical and experimental free surface elevations for case C.

numerical wave tank is 10 m long and 2 m wide with a water depth of 0.505 m. The cylinder is placed at 5.5 m. The experimental wave gage was located directly upstream of the vertical cylinder in the center of the basin and is used for comparison with the free surface obtained by REEF3D. A Cartesian grid is implemented in the model i.e. $dx = dy = dz$=0.025m to discretize the numerical wave tank with 1,280,000 cells. The cells are distributed as 400, 80 and 40 in the $x, yandz$ directions, respectively. The 3D cases have been run on a 12-core workstation. For case C, the run is performed with the given focus point and time. Figs. 5 and 6 show the comparison of numerical and experimental results for free surface elevations and wave forces on the cylinders, respectively for case C. Due to the prevailing linearity of this case, good agreement for the free surface upstream of the cylinder can be achieved in this configuration (Fig. 5). Also, the inline wave forces on the cylinder are predicted well (Fig. 6).

Case D has a larger input focus wave amplitude A_F. Numerical simulations show, that due to the large non-linearity, the focus point is located further downstream than the intended value for x_F. Based on the actual focus point, x_F is reduced in such away, that the actual focus point is moved back to the front of the cylinder. Figs. 7 and 8 show the comparison of numerical and experimental results for free surface elevations and wave forces on the cylinders,

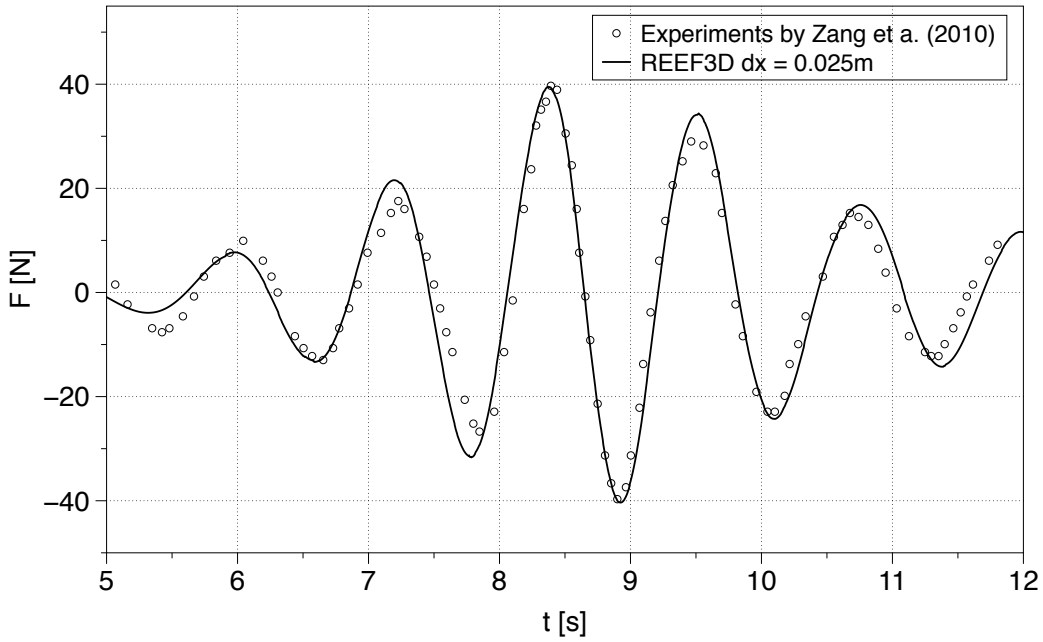

Figure 6: Comparison of numerical and experimental wave forces on the vertical circular cylinder for case C.

respectively for case D. With this adjustment, the computed free surface agrees well with the measured data (Fig. 7). The magnitude and the shape of inline force graph is also predicted well (Fig. 8).

4.3 Free Surface Flow Features During the Interaction

The interaction of the focused wave with the cylinder modifies the kinematics and the flow field around it. Here, the higher wave steepness case (case D) is considered for further study. Fig. 9 shows the free surface with velocity magnitude when the focused wave interacts with the cylinder for different time instants for case D. First, the focused wave trough followed by the lower part of the wave crest interacts with the cylinder causing a rise of water level in front of the cylinder at t=8.0 s. Thus, the wave crest velocity increases in the vicinity of the cylinder (Fig. 9 (a)). At t=8.0 s, the wave just focuses in front of the cylinder and the focused wave front impacts the cylinder as show in Fig. 9 (a) and (b) resulting in increased water levels on both sides of the cylinder and consequently, this strongly affects the velocity field (Fig. 9 (c) and (d)). As the focused wave crest propagates further, a small water jet is developed in the downstream side of the cylinder as the focused wave crest passes the cylinder as seen in Fig. 9 (c) and (d). The small downstream side water jet is formed behind cylinder during the interaction of the steep focused wave crest with the cylinder and it is separated upstream by the cylinder during the interaction. The separated wave fronts rush downstream around the cylinder and they colloid each other behind the cylinder developing a small water jet along the center line of the cylinder in the wave direction. As reported by Alagan Chella et al. (2016) and Kamath et al (2016), the size of the downstream water jet increases as the amplitude of the incident wave becomes larger.

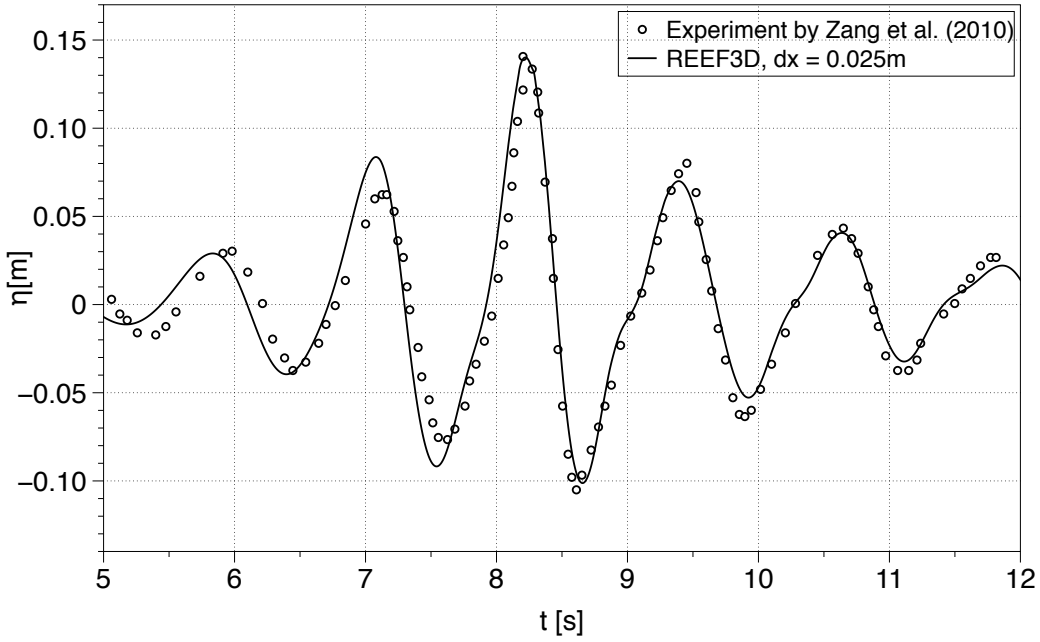

Figure 7: Comparison of numerical and experimental free surface elevations for case D.

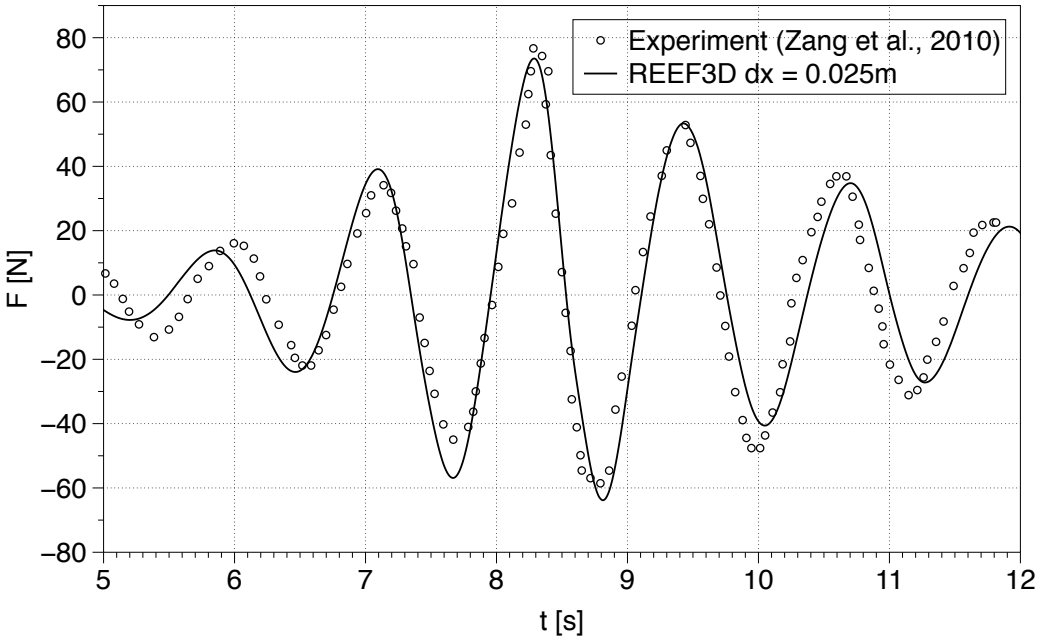

Figure 8: Comparison of numerical and experimental wave forces on the vertical circular cylinder for case D.

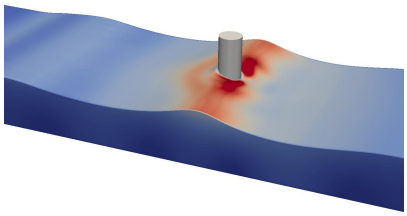

(a) t=8.0s

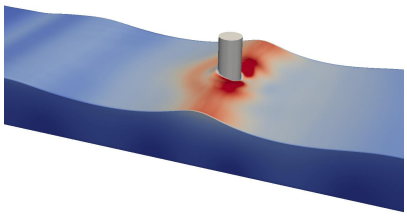

(b) t= 8.2s

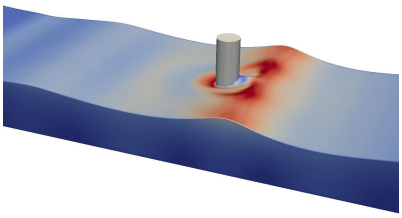

(c) t= 8.4s

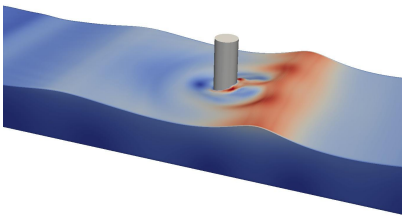

(d) t= 8.6s

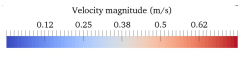

Figure 9: Simulated free surfaces with velocity magnitude (m/s) during the interaction for different time instants for case D.

In order to investigate the changes in the free surface elevations during and after the focused wave interaction with the cylinder, the numerically captured free surface elevation contours (plan view) are examined. Fig. 10 depicts the variation in the free surface elevations during the interaction process. As mentioned in Sec. 4.2, the intended focus point is just in front of the cylinder and the lower part of wave crest first interacts with the cylinder at t=8.0s (Fig. 9 (b)). Then, the part of the wave crest along the width of the wave tank grows higher around the surface of the cylinder (Fig. 10 (a)). An increase in the free surface elevation in front and at the sides of the cylinder is noticed as the wave crest further propagates along the cylinder as seen in (Fig. 10 (b)). When the wave crest passes the cylinder, it creates a small downstream water jet just behind the cylinder in the shadow region is clearly visible in (Fig. 9 (d) and Fig. 10 (c)). This free surface feature disappears as the wave crest travels farther from the cylinder (Fig. 10 (d)). The free surface flow features behind the cylinder would become more important for a group of cylinders particularly in the case of a group of closely spaced cylinders e.g. multi-leg supported offshore structures. The influence of the downstream water jet on wave forces on tandem cylinders has been investigated numerically by Bihs et al. (2016). They studied the breaking wave interaction with a pair of cylinders placed in tandem at different separation distances for different wave impact scenarios.
Interestingly, strong free surface flow features are noticed when the wave crest following the intended focused wave crest interacts with the cylinder as depicted in Fig. 11. The flow field is disturbed along the wave propagation direction due to the interaction of the focused wave crest with the cylinder. Further, the subsequent wave crest right after the focused wave crest interacts with the disturbed free surface before reaching the cylinder (Fig. 11 (a)). As a result, wave diffraction occurs and the diffraction patterns including semi-circular waves around the cylinder are clearly seen in Fig. 11 (b). Finally, the semi-circular wave patterns cease as the second wave crest leaves the cylinder further downstream. The numerical model is capable of capturing the free surface flow features during the interaction of focused wave with the cylinder.

4.4 Breaking Focused Waves

A breaking focused wave is simulated over a constant water depth of d=0.80m with H_s=0.015m and T_p=1.40s. In the present case, the focused wave generation is based on the constant steepness method proposed by Rapp and Melville Rapp and Melville (1990) with a total of 28 wave components. With this approach, a very steep wave crest can be achieved by focusing all the wave components at a particular point in space and time. Fig. 12 shows the evolution of the free surface elevation at different time instants along the numerical wave tank. First, the focused wave group starts to evolve as the wave components started to interact with each other. The height of the focused wave and the slope of the wave front increase continuously as the wave group propagates further forward in the wave tank. Then the focused wave crest breaks at x=5.8m after attaining the maximum breaker height H_b=0.385m with a very steep wave front as depicted in Fig. 12. Particularly, the evolution of the focused wave group up to breaking also resembles the scenario of a regular wave approaches the breaking point. After the breaking point, the energy content of the wave group decreases and thus, the height of the wave group decreases continuously shoreward. The computed wave surface elevation at breaking is presented in Fig. 13. During the wave group approaching the breaking point, the focused wave crest evolves with a steeper wave front and a following deeper wave trough. Moreover, the wave amplitude at the breaking point is 0.285m which is much larger than the

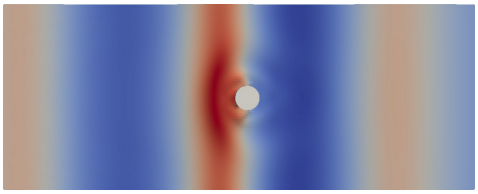

(a) t= 8.0s

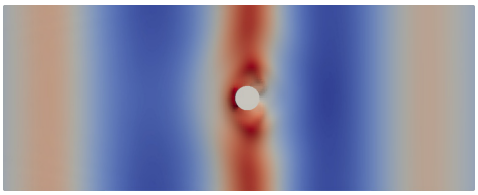

(b) t= 8.2s

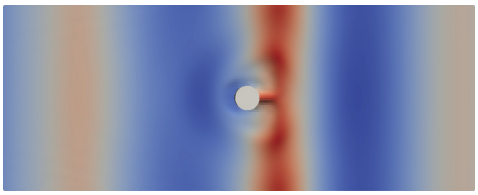

(c) t= 8.4s

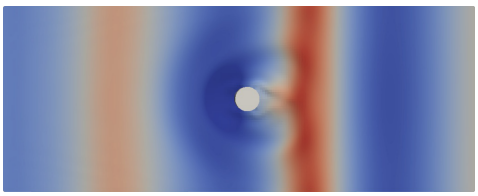

(d) t= 8.6s

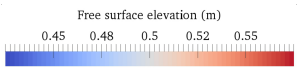

Figure 10: Modeled free surface flow features with free surface elevation (m) variation during the focused wave interaction with the cylinder for different time (t) instants for case D.

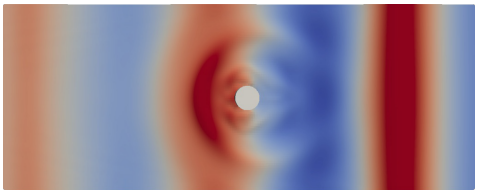

(a) t= 9.2s

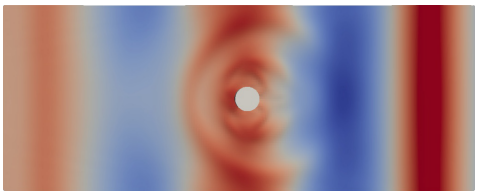

(b) t= 9.4s

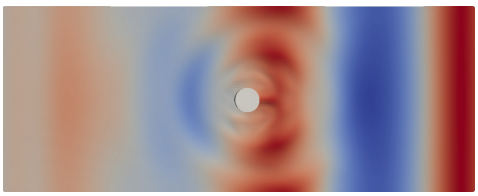

(c) t= 9.6s

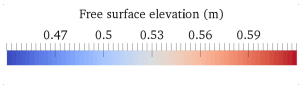

Figure 11: Modeled free surface flow features with free surface elevation (m) variation after the focused wave interaction with the cylinder for different time (t) instants for case D.

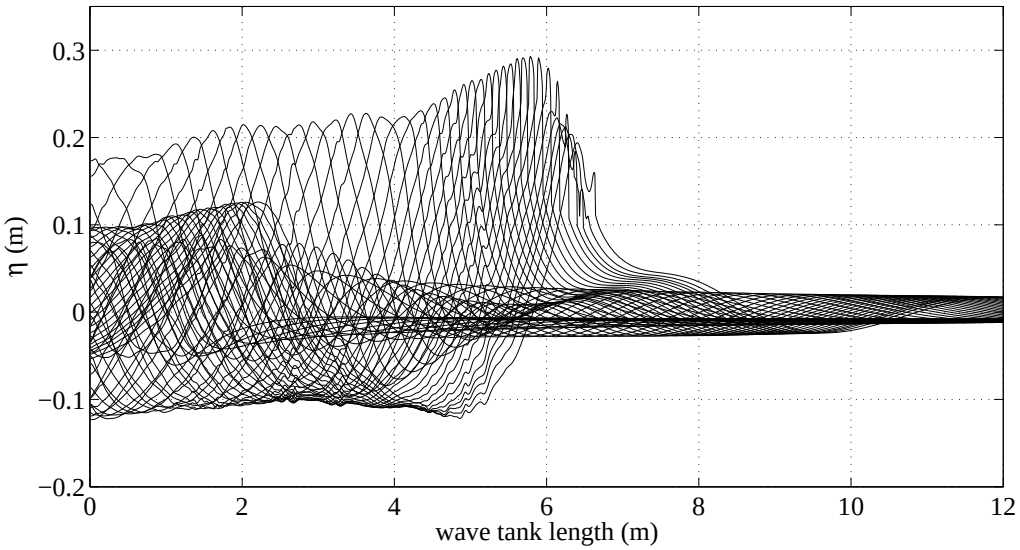

Figure 12: Simulated wave surface elevations along the wave tank for the breaking focused wave case.

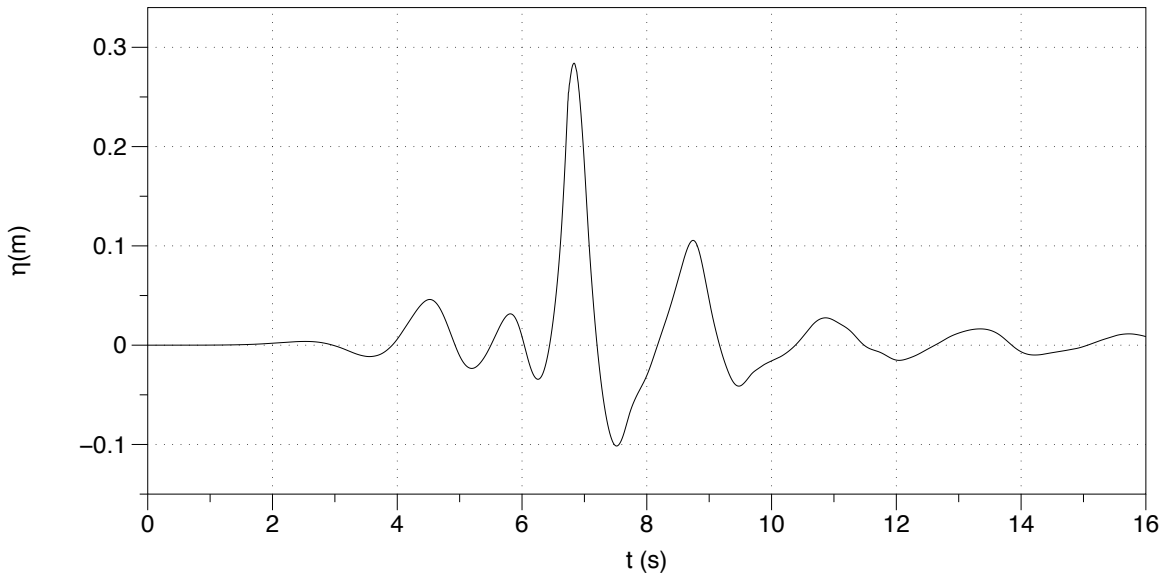

Figure 13: Simulated wave surface elevation at x=5.80m for the breaking focused wave case.

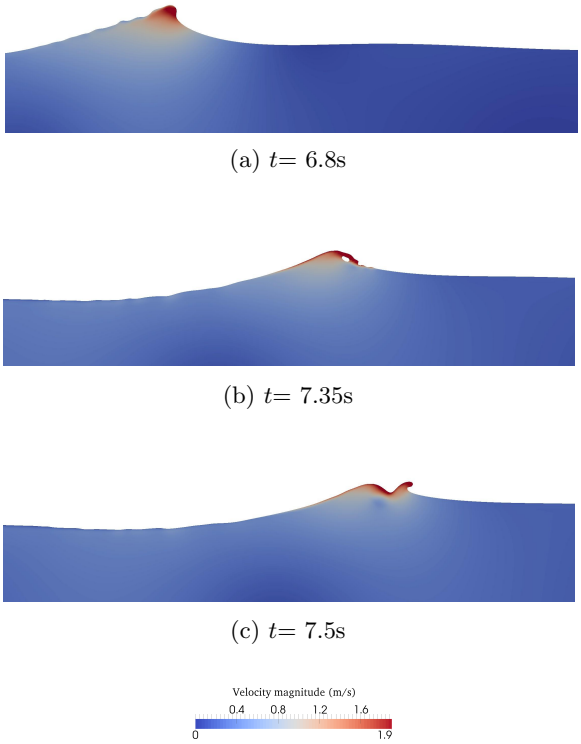

(a) t= 6.8s

(b) t= 7.35s

(c) t= 7.5s

Figure 14: Simulated free surface profiles with velocity magnitude (m/s) during the breaking process for different time (t) instants.

focus amplitude of the steepest case (case D, A_f=0.07m).

Fig. 14 presents the free surface flow features during the breaking process at different time instants. The breaking point is recognized when the most part of the wave front becomes vertical as shown in Figs. 14 (a) and 12 . When the focused wave height increases further, the steep wave crest overturns forward and fall on the preceding water surface creating a small encased air pocket inside the wave crest (Fig. 14 (b)). As a result, the splash-up occurs with the secondary wave crest (Fig. 14 (c)). Importantly, the velocity magnitude of the secondary wave crest is as larger as the velocity of the focused wave crest. The significant free surface flow features during the breaking process including the developement of overturning wave crest and air pocket and the splash-up are represented well in the numerical simulations. Moreover, the computed free surface profiles during the breaking process are similar to the flow characteristics of breaking regular waves in shallow waters Alagan Chella et al. (2016*b*); Ting and Kirby (1994); Basco (1985).

5 CONCLUSIONS

Focused wave kinematics and focused wave-structure interaction have been investigated numerically with the three-dimensional Navier-Stokes solver REEF3D. The flow was modeled as a two-fluid flow system with the level set method for the capturing of the interface. The numerical model is validated for simulating the focused waves and their interaction with a

vertical cylinder against the experimental data by Ning et al. Ning et al. (2009) for kinematics and Zang et al. Zang et al. (2010) for wave-structure interaction. The simulated results are in good agreement with the experimental data for free surface elevation at the focus point and focused wave force on the cylinder. For the higher wave steepness cases, the focus point location is strongly influenced by the wave non-linearity which evolves from the interaction of the wave components during the evolution of the wave group. It is seen that the intended focus point location moves forward in the direction of the propagation as the focus wave amplitude is increased. Further, the changes in the kinematics and the free surface flow features are investigated for the higher steepness case. During the interaction, the focused wave crest develops a small water jet on the downstream behind the cylinder and this disappears after the wave crest propagates further downstream in the wave direction. The interaction of the subsequent wave crest after the focused wave with the cylinder creates strong diffraction patterns including noticeable semi-circular waves in the vicinity of the cylinder. Further, the kinematics of the breaking focused wave is studied. The evolution of the focused wave group up to the breaking point is found have a similar trend as a breaking regular wave. In addition, the development of the free surface profiles are represented well in the numerical simulations. Overall, the open-source CFD model REEF3D showed good performance for the simulation of focused wave propagation and interaction with a vertical cylinder and breaking focused waves. For future studies, the interaction of focused breaking waves with a structure will be investigated to further explore the possibilities of the advanced CFD tool and obtain more insights into the interaction of extreme waves with offshore structures.

ACKNOWLEDGEMENTS

The research work has been funded by the Research Council of Norway through the project "Hydrodynamic Loads on Offshore Wind Turbine Substructures" (project number: 246810).

References

Afzal, M.S., Bihs, H., Kamath, A. and Arntsen, Ø.A. (2015). Three-dimensional numerical modeling of pier scour under current and waves using level-set method. *Journal of Offshore Mechanics and Arctic Engineering*, **137**, 32001–32007.

Alagan Chella, M., Bihs, H., Myrhaug, D. and Muskulus, M. (2015a). Breaking characteristics and geometric properties of spilling breakers over slopes. *Coastal Engineering*, **95**, 4–19.

Alagan Chella, M., Bihs, H., Myrhaug, D. and Muskulus, M. (2016*a*). Breaking solitary waves and breaking wave forces on a vertically mounted slender cylinder over an impermeable sloping seabed. *Journal of Ocean Engineering and Marine Energy*. DOI: 10.1007/s40722-016-0055-5.

Alagan Chella, M., Bihs, H., Myrhaug, D. and Muskulus, M. (2016*b*). Hydrodynamic characteristics and geometric properties of plunging and spilling breakers over impermeable slopes. *Ocean Modelling*, **103**, 53–72.

Baldock, T.E., Swan, C. and Taylor, P.H. (1996). A laboratory study of nonlinear surface waves on water. *Philosophical Transactions: Mathematical, Physical and Engineering Sciences*, **354**(1707), 649–676.

Basco, D.R. (1985). A qualitative description of wave breaking. *J. Waterw. Port Coast. Ocean Eng.*, **3**(2), 171–188.

Berthelsen, P.A. and Faltinsen, O.M. (2008). A local directional ghost cell approach for incompressible viscous flow problems with irregular boundaries. *Journal of Computational Physics*, **227**, 4354–4397.

Bihs, H., Kamath, A., Alagan Chella, M., Aggarwal, A. and Arntsen, Ø.A. (2016*a*). A new level set numerical wave tank with improved density interpolation for complex wave hydrodynamics. *Computers and Fluids*, **140**, 191–208.

Bihs, H., Kamath, A., Alagan Chella, M. and Arntsen, Ø.A. (2016*b*). Breaking wave interaction with tandem cylinders under different impact scenarios. *J. Waterw. Port Coast. Ocean Eng.* DOI: 10.1061/(ASCE)WW.1943-5460.0000343.

Bihs, H., Ong, M.C., Kamath, A. and Arntsen, Ø.A. (2012). A level set method based numerical wave tank for the calculation of wave forces on horizontal and vertical cylinders. *MekIT'13, Trondeim, Norway.*

Chaplin, J.R., Rainey, R.C.T. and Yemm, R.W. (1997). Ringing of a vertical cylinder in waves. *Journal of Fluid Mechanics*, **350**, 119–147.

Chen, L.F., Zang, J., Hillis, A.J., Morgan, G.C.J. and Plummer, A.R. (2014). Numerical investigation of wave–structure interaction using openFOAM. *Ocean Engineering*, **88**, 91—109.

Chorin, A. (1968). Numerical solution of the Navier-Stokes equations. *Mathematics of Computation*, **22**, 745–762.

Jiang, G.S. and Shu, C.W. (1996). Efficient implementation of weighted ENO schemes. *Journal of Computational Physics*, **126**, 202–228.

Kamath, A., Alagan Chella, M., Bihs, H. and Arntsen, Ø.A. (2015*a*). CFD investigations of wave interaction with a pair of large tandem cylinders. *Ocean Engineering*, **108**, 738–748.

Kamath, A., Bihs, H., Alagan Chella, M. and Arntsen, Ø.A. (2016). Breaking wave interaction with a vertical cylinder and the effect of breaker location. *Ocean Engineering*, **128**, 105–115.

Kamath, A., Bihs, H. and Arntsen, Ø.A. (2015*b*). Numerical investigations of the hydrodynamics of an oscillating water column. *Ocean Engineering*, **102**, 40–50.

Le, H. and Moin, P. (1991). An improvement of fractional step methods for the incompressible navier-stokes equations. *Journal of Computational Physics*, **92**, 369–379.

Mayer, S., Garapon, A. and Sørensen, L.S. (1998). A fractional step method for unsteady free surface flow with applications to non-linear wave dynamics. *International Journal for Numerical Methods in Fluids*, **28**, 293–315.

Ning, D.Z., Zang, J., Liu, S.X., Eatock Taylor, R., Teng, B. and Taylor, P.H. (2009). Free-surface evolution and wave kinematics for nonlinear uni-directional focused wave groups. *Ocean Engineering*, **36**, 1226—1243.

Osher, S. and Sethian, J.A. (1988). Fronts propagating with curvature-dependent speed: Algorithms based on Hamilton-Jacobi formulations. *Journal of Computational Physics*, **79**, 12–49.

Paulsen, B.T., Bredmose, H. and Bingham, H. (2014). An efficient domain decomposition strategy for wave loads on surface piercing circular cylinders. *Coastal Engineering*, **86**, 57–76.

Rapp, R.J. and Melville, W. (1990). Laboratory measurements of deep-water breaking waves. *Philosophical Transactions: Mathematical, Physical and Engineering Sciences*, **331**(1622), 735–800.

Schäffer, H.A. (1996). Second-order wavemaker theory for irregular waves. *Ocean Engineering*, **23**(1), 47–88.

Shu, C.W. (1997). Essentially non-oscillatory and weighted essentially non-oscillatory schemes for hyperbolic conservation laws. Technical report, Institute for Computer Applications in Science and Engineering (ICASE).

Shu, C.W. and Osher, S. (1988). Efficient implementation of essentially non-oscillatory shock capturing schemes. *Journal of Computational Physics*, **77**, 439–471.

Soomere, T. (2010). Rogue waves in shallow water. *The European Journal of Special Topics*, **185**, 81–96.

Stansell, P. (2004). Distributions of freak wave heights measured in the north sea. *Applied Ocean Research*, **26**(1-2), 35—48.

Sussman, M., Smereka, P. and Osher, S. (1994). A level set approach for computing solutions to incompressible two-phase flow. *Journal of Computational Physics*, **114**, 146–159.

Ting, F.C.K. and Kirby, J.T. (1994). Observation of undertow and turbulence in a laboratory surf zone. *Coast. Eng.*, **24**(1-2), 51–80.

van der Vorst, H. (1992). BiCGStab: A fast and smoothly converging variant of Bi-CG for the solution of nonsymmetric linear systems. *SIAM Journal of Scientific Computing*, **13**, 631–644.

Westphalen, J., Greaves, D.M., Williams, C.J.K., Hunt-Raby, A.C. and Zang, J. (2012). Focused waves and wave-structure interaction in a numerical wave tank. *Ocean Engineering*, **45**, 9–21.

Zang, J., Taylor, P.H. and Tello, M. (2010). Steep wave and breaking wave impact on offshore wind turbine foundations - ringing re-visited. *25th International Workshop on Water Waves and Floating Bodies, Harbin, China.*